The Astronomical Journal, 155:2 (13pp), 2018 January https://doi.org/10.3847/1538-3881/aa9930

The Dynamical History of 2060 Chiron and Its Proposed Ring System

Jeremy Wood[1,2], Jonti Horner[2,3], Tobias C. Hinse[4], and Stephen C. Marsden[2]

[1] Hazard Community and Technical College, 1 Community College Drive, Hazard, KY 41701, USA; jeremy.wood@kctcs.edu

[2] University of Southern Queensland, Computational Engineering and Science Research Centre, West Street, Toowoomba, QLD 4350, Australia

[3] Australian Centre for Astrobiology, UNSW Australia, Sydney, NSW 2052, Australia

[4] Korea Astronomy and Space Science Institute, 776 Daedukdae-ro, Yuseong-gu, Daejeon 305-348, Republic of Korea

Received 2017 September 2; revised 2017 November 6; accepted 2017 November 6; published 2017 December 7

Abstract

The surprising discovery of a ring system around the Centaur 10199 Chariklo in 2013 led to a reanalysis of archival stellar occultation data for the Centaur 2060 Chiron by Ortiz et al. One possible interpretation of that data is that a system of rings exists around Chiron. In this work, we study the dynamical history of the proposed Chiron ring system by integrating nearly 36,000 clones of the Centaur backward in time for 100 Myr under the influence of the Sun and the four giant planets. The severity of all close encounters between the clones and planets while the clones are in the Centaur region is recorded, along with the mean time between close encounters. We find that severe and extreme close encounters are very rare, making it possible that the Chiron ring system has remained intact since its injection into the Centaur region, which we find likely occurred within the past 8.5 Myr. Our simulations yield a backward dynamical half-life for Chiron of 0.7 Myr. The dynamical classes of a sample of clones are found. It is found that, on average, the Centaur lifetimes of resonance hopping clones are twice those of random-walk clones because of resonance sticking in mean motion resonances. In addition, we present MEGNO and chaotic lifetime maps of the region bound by 13 au $\leqslant a \leqslant$ 14 au and $e \leqslant 0.5$. We confirm that the current mean orbital parameters of Chiron are located in a highly chaotic region of $a - e$ phase space.

Key words: minor planets, asteroids: individual (2060 Chiron) – planets and satellites: dynamical evolution and stability – planets and satellites: rings

1. Introduction

The study of small bodies of the solar system was changed forever in 1977, with the discovery of a large icy object moving on an orbit between those of Saturn and Uranus (Kowal et al. 1979). That object was subsequently named Chiron. It was soon realised that its orbit was dynamically unstable, with a mean half-life of 0.2 Myr, which is far shorter than the age of the solar system (e.g., Oikawa & Everhart 1979; Hahn & Bailey 1990). For more than a decade, 2060 Chiron was an oddity—but following the discovery of 5145 Pholus in 1992, a growing population of such objects in the outer solar system has been discovered—a population now known as the Centaurs.

Over the years, a number of different schemes have been proposed to define Centaurs (e.g., Horner et al. 2003; Elliot et al. 2005; Chiang et al. 2007; Gladman et al. 2008). Across all these schemes, it can be generally said that Centaurs have orbits between the giant planets Jupiter and Neptune. For this work, we follow the definition used by the Minor Planet Center, which considers objects to be Centaurs if they move on orbits with perihelia beyond the orbit of Jupiter and with semimajor axes within the orbit of Neptune.[5] Those objects in this region that are trapped in 1:1 resonance with one of the giant planets (the Trojans) are excluded from the list, and are not considered to be Centaurs. Using this definition, more than 220 objects can presently be classified as Centaurs.[6]

The Centaurs move on highly chaotic orbits that are frequently perturbed by the gravitational influence of the four giant planets. The strongest perturbations typically occur as a result of close approaches between the Centaurs and those planets (e.g., Marsden 1962; Horner et al. 2004b). The instability of the Centaur region is exemplified by the fact that Centaurs have dynamical lifetimes and half-lives much less than the age of the solar system, with values typically $\ll$100 Myr (Dones et al. 1996; Levison & Duncan 1997; Tiscareno & Malhotra 2003; Horner et al. 2004a; Di Sisto & Brunini 2007; Bailey & Malhotra 2009; Pál et al. 2015).

It is therefore clear that these objects are ephemeral in nature, and that their ranks must be replenished over time from other sources. Proposed source populations for the Centaurs include the Oort Cloud (Emel'yanenko et al. 2005; Brasser et al. 2012; de la Fuente Marcos & de la Fuente Marcos 2014; Fouchard et al. 2014), the Jupiter Trojans (Horner et al. 2004a; Horner & Wyn Evans 2006; Horner et al. 2012b), the Neptune Trojans (Horner & Lykawka 2010; Lykawka & Horner 2010; Horner et al. 2012a), the Scattered Disk (Di Sisto & Brunini 2007; Volk & Malhotra 2008), and other populations in the Edgeworth-Kuiper Belt (Levison & Duncan 1997; Volk & Malhotra 2008). Of these many source regions, it is thought that the majority of Centaurs originate within the Scattered Disk (Di Sisto & Brunini 2007; Volk & Malhotra 2008).

After these small bodies escape from one of the more stable source populations into the Centaur region, they will typically spend on the order of $\sim 10^6$ years as a Centaur before diffusing out of that region (Tiscareno & Malhotra 2003). The final fates of Centaurs are varied—some will collide with the Sun or one of the planets, or will be torn apart by tidal forces during a planetary close encounter, while others will be thrown onto orbits beyond Neptune or will be ejected from the solar system entirely (Noll 1994; Horner et al. 2004a; Volk & Malhotra 2008; Wood et al. 2016).

[5] http://www.minorplanetcenter.net/iau/lists/Unusual.html (accessed 2016 December 17).

[6] http://www.minorplanetcenter.net/iau/lists/t_centaurs.html (accessed 2017 October 8).

During the course of their evolution, studies have shown that at least one-third of the Centaurs will evolve onto cometary orbits with perihelia in the inner solar system (Horner et al. 2004b; Jewitt 2004; Bailey & Malhotra 2009). As such, the Centaurs are generally regarded as the principal parent population for the short period comets (Tiscareno & Malhotra 2003; Groussin et al. 2004; Horner et al. 2004a; Volk & Malhotra 2008; Bailey & Malhotra 2009; Jewitt 2009; Kovalenko et al. 2011).

Indeed, several Centaurs (including Chiron) have been observed exhibiting cometary activity (e.g., Jewitt 2009; Shi & Ma 2015; Wierzchos et al. 2017). Given the extreme dynamical instability exhibited by the Centaurs, coupled with the frequent close encounters they experience with the giant planets, the discovery in 2013 of a system of rings orbiting the Centaur 10199 Chariklo came as a huge surprise (Braga-Ribas et al. 2014). Those rings, revealed by unexpected dimmings of a star occulted by Chariklo prior to and immediately after the occultation event, are narrow and dense, and lie at radii of ~391 and ~405 km.

It is still unknown whether the rings formed recently, or predate Chariklo's injection into the Centaur region, though rings have also recently been discovered around the dwarf planet Haumea (Ortiz et al. 2017), which orbits beyond Neptune. This suggests that rings around small bodies could form in the Trans-Neptunian region.

Furthermore, a recent dynamical study has shown that such rings could readily survive with Chariklo through its entire evolution in the Centaur region, since sufficiently close encounters to disrupt the rings are rare (Wood et al. 2017).

The chance discovery of Chariklo's ring system prompted a reanalysis of stellar occultation data obtained for 2060 Chiron in 1993, 1994, and 2011 by Ortiz et al. (2015). The original analysis of that occultation data found dips in the light curve that, it was thought, corresponded to regions outside the nucleus, which were then interpreted as comet-like dust jets (Elliot et al. 1995; Bus et al. 1996) or symmetrical jet-like features (Ruprecht et al. 2015). The recent reanalysis of this data suggests that it might also be interpreted as evidence for a ring system similar to that of Chariklo, with a mean radius of 324 ± 10 km (Ortiz et al. 2015).

The origin of this proposed ring structure could be the result of a tidal disruption of Chiron due to a close encounter with a planet (Hyodo et al. 2016), a collision between Chiron and another body (Melita et al. 2017), a collision between an orbiting satellite and another body (Melita et al. 2017), the tidal disruption of an orbiting satellite (El Moutamid et al. 2014), or debris ejected from Chiron itself due to cometary activity (Pan & Wu 2016).

Over time, rings can widen due to viscous spreading (Michikoshi & Kokubo 2017). This process can occur on timescales as short as hundreds of years. However, the extent of the rings can be constrained, keeping them far more narrow, if shepherd satellites are present (French et al. 2003; Jacobson & French 2004; El Moutamid et al. 2014; Michikoshi & Kokubo 2017). At the present time no shepherd satellites are known to exist orbiting any Centaur, and hence their possible dynamical role will not be considered in this study.

Given the extreme dynamical instability exhibited by Chiron, it is interesting to consider whether its ring system could survive through the entirety of its life as a Centaur. If deep close encounters with the giant planets are sufficiently frequent, then it might be possible to place a constraint on the age of any rings around Chiron on the basis of its past dynamical history.

Table 1
The Orbital Elements of Chiron for Epoch 2457600.5 JD

Property	Value	Units
a	$13.639500 \pm (1.48 \times 10^{-6})$	au
e	$0.38272700 \pm (9.62 \times 10^{-8})$	…
i	$6.947000 \pm (6.67 \times 10^{-6})$	deg
Ω	$209.21600 \pm (6.05 \times 10^{-5})$	deg
ω	$339.53700 \pm (6.19 \times 10^{-5})$	deg
M	$145.97800 \pm (2.97 \times 10^{-5})$	deg

Note. Based on an observational arc length of 44,305.9 days taken from the asteroids dynamic site (accessed 2015 December 31). Here, a is the semimajor axis, e is the eccentricity, and i is the inclination of the orbit. Ω, ω, and M are the longitude of ascending node, argument of perihelion, and mean anomaly, respectively. Each uncertainty is the standard deviation around the best-fit solution.

As a result, in this work, we follow Wood et al. (2017), and examine the dynamical history of Chiron and its proposed ring system. In doing so, we explore the likelihood that its rings could be "primordial" (i.e., could date back to before the object was captured as a Centaur) barring ring dispersal by viscous spreading. Our results also allow us to explore the likely source population of Chiron, and to confirm its status as one of the most dynamically unstable Centaurs.

In Section 2, we present the physical and orbital properties of 2060 Chiron. In Section 3, we discuss the means by which we can measure the severity of close encounters between ringed small bodies and planets, and in Section 4, we discuss the two dynamical classes that have been proposed for the Centaurs. We present our methodology in Section 5, and then present and discuss the results of our numerical integrations of Chiron in Section 6. Finally, in Section 7, we present our conclusions and discuss possible directions for future work.

2. The Properties of 2060 Chiron

2.1. Orbital Properties

After Chiron was discovered, pre-discovery images dating back as early as the late 19th century allowed its orbit to be well constrained (Liller et al. 1977; Kowal et al. 1979). It was soon found that the orbit of Chiron was unlike the orbit of any known small body at the time. Its aphelion lay between Saturn and Uranus, while its perihelion lay just interior to Saturn's orbit.

Since its discovery, more observations of Chiron have allowed its orbit to be even further refined. The current best-fit orbital properties of Chiron are shown in Table 1 and were taken from the Asteroids Dynamic site (Knezevic & Milani 2012).

Using the semimajor axis, a, and eccentricity, e, from Table 1, the perihelion and aphelion distances are found to be 8.4 au and 18.86 au, respectively. The semimajor axis is about 0.01 au away from the interior 5:3 mean motion resonance of Uranus located at about 13.66 au. The eccentricity of Chiron's orbit lies in the middle of the eccentricity range for the orbits of the known Centaurs, 0.01–0.73,[7] and is high enough to cause Chiron to cross the orbits of both Saturn and Uranus. These

[7] http://www.minorplanetcenter.net/iau/lists/Centaurs.html (accessed 2017 August 9).

giant-planet perturbations and close approaches have a significant effect on the dynamical evolution of Chiron's orbit (Oikawa & Everhart 1979; Scholl 1979; Kovalenko et al. 2002), which is reflected in the relatively short dynamical lifetime of ~1 Myr (Hahn & Bailey 1990; Horner et al. 2004a).

Furthermore, the half-life of its orbit is 1.03 Myr in the forward direction and 1.07 Myr in the backward direction (Horner et al. 2004a). Both times are much less than the age of the solar system.

The instability of Chiron's current orbit makes it highly unlikely that its orbit is primordial. Instead, the general consensus is that Chiron follows a chaotic orbit and originated in the Kuiper Belt (Oikawa & Everhart 1979; Hahn & Bailey 1990; Lazzaro et al. 1996; Silva & Cellone 2001; Duffard et al. 2002; Kovalenko et al. 2002).

Using the taxonomy of Horner et al. (2003), Chiron is classified as an object in the SU_{IV} class. This means that its dynamics are controlled by Saturn at perihelion and by Uranus at aphelion. The subscript IV means that the Tisserand parameter with respect to Saturn is >2.8 (Horner et al. 2003). The Tisserand parameter, T_p, is a quantity calculated from the orbital parameters of a small body and those of a planet it could encounter. It is defined by

$$T_p = \frac{a_p}{a} + 2\cos(i - i_p)\sqrt{\frac{a}{a_p}(1 - e^2)} \quad (1)$$

(e.g., Murray & Dermott 1999). Here, a_p is the semimajor axis of a planetary orbit, i is the inclination of the small body orbit, and i_p is the inclination of the planetary orbit.

To first order, the Tisserand parameter of an orbit with respect to a given planet is expected to be conserved through an encounter with that planet, with the precise value giving an indication of the maximum strength of encounters that are possible with that planet.

Broadly, if $T_p > 3$, then particularly close encounters are not possible between the two objects, while for $2.8 \leqslant T_p \leqslant 3$, extremely close encounters can occur that might lead to the object being ejected from the solar system in a single pass (Horner et al. 2003).

2.2. Density, Size, and Mass

Unlike the relatively high precision with which the orbital parameters of Chiron are known, the physical properties remain much more poorly constrained. The diameter of Chiron has had to be estimated based on an assumed albedo. Though a strong effort to determine the size of Chiron has been made over the past 2 decades, efforts have been hampered by the interference from possible material located outside the nucleus, cometary activity, and Chiron's elongated shape (Fornasier et al. 2013; Ortiz et al. 2015).

Radius measurements ranging from 71 km (Groussin et al. 2004) to a constraint of <186 km (Sykes & Walker 1991) have been reported. Ortiz et al. (2015) report an overall average effective spherical radius of 90 km, which we adopt for this work.

Because of the large uncertainty in the size and mass of Chiron, Chiron's overall density is also poorly known. Meech et al. (1997), in their study of a coma around Chiron, report a bulk density in the range 500–1000 kg m^{-3}. Using a spherical radius of 90 km, this corresponds to a mass range of 1.53×10^{18} kg –3.05×10^{18} kg.

Table 2
A Scale Ranking the Severity of a Close Encounter between a Ringed Small Body and a Planet Based on the Minimum Distance Obtained between the Small Body and the Planet, d_{min}, during the Close Encounter

d_{min} Range	Severity
$d_{min} \geqslant R_H$	Very low
$R \leqslant d_{min} < R_H$	Low
$R_{td} \leqslant d_{min} < R$	Moderate
$R_{roche} \leqslant d_{min} < R_{td}$	Severe
$d_{min} < R_{roche}$	Extreme

Note. R_H, $R = 10R_{td}$, R_{td}, and R_{roche} are the Hill radius of the planet with respect to the Sun, ring limit, tidal disruption distance, and roche limit, respectively.

3. Measuring the Severity of Close Encounters with Planets

Currently it is unknown what role, if any, the sporadic activity of Chiron played in the formation of any ring structure around the body. Rings could have formed either before or after Chiron entered the Centaur region. But given that Chiron presently lies in a chaotic and unstable orbit prone to planetary close encounters, it is of interest to determine the likelihood that such encounters could severely damage or destroy any orbiting ring structure.

To accomplish this, a method to gauge the severity of such an encounter is needed. Primarily, the severity of a close encounter between a ringed small body and a planet is determined by the minimum approach distance between the small body and planet, d_{min}.

If the small body is in a parabolic or hyperbolic orbit relative to the planet (it has not been captured as a satellite), then the velocity at infinity of the small body relative to the planet also plays a role in determining the encounter severity, albeit to a lesser extent than the depth of the encounter.

Wood et al. (2017) ignored velocity effects and developed a severity scale based on d_{min} relative to the Hill radius, R_H; tidal disruption distance, R_{td}; the ring limit, $R = 10R_{td}$; and the Roche limit, R_{roche}. This scale is shown in Table 2.

The Hill radius defines a sphere of influence centered on a secondary body of mass m_s in an orbit with orbital radius R_{radial} around a primary body of mass M_p in the planar problem. The Hill radius is approximately given by

$$R_H \approx R_{radial}\left(\frac{m_s}{3M_p}\right)^{\frac{1}{3}} \quad (2)$$

(e.g., Murray & Dermott 1999). For non-circular orbits, R_{radial} is approximated using the semimajor axis of the orbit. Loosely defined, the Hill radius is the distance around a secondary body (relative to a primary body) within which satellites can orbit without their orbits being completely disrupted by tidal forces due to the primary body. In the case where the secondary body is a planet and the primary body the Sun, it is found that all known planetary satellites follow this rule, being contained well within the Hill spheres of their host planets. For other objects moving in the system, the Hill radius of a planet can be used to indicate the region of space around its orbit, into which other objects move at their peril.

Typically encounters at a distance greater than ~3 Hill radii will have only a limited effect on the long-term stability of an object, while orbits that approach within this distance are

typically dynamically unstable, unless close approaches are prevented by mutual mean motion resonances between the objects concerned (e.g., Williams & Benson 1971; Malhotra 1995; Horner et al. 2011; Robertson et al. 2012; Wittenmyer et al. 2012).

The ring limit is a relatively new critical distance introduced by Araujo et al. (2016) and used by Wood et al. (2017) to examine the stability of Chariklo's ring system against close encounters. It is loosely defined as lying at 10 tidal disruption distances from a given planet, and represents an upper limit on the minimum approach distance for close encounters for which the effect on a ring of a minor body is just noticeable (meaning the maximum change in orbital eccentricity of the orbit of any ring particle = 0.01). Here we apply the ring limit to study the influence of close encounters between Chiron and the giant planets.

Given a typical solar system small body, the tidal disruption distance, $R_{\rm td}$, lies well within the Hill radius for a given planet. When the separation between a small body and a planet is closer than $R_{\rm td}$, a secondary body-satellite binary pair of total mass $m_s + m_{\rm sat}$ and semimajor axis a_B can be permanently disrupted by tidal forces in one pass. It should be noted in passing that as defined in this manner, the ring limit and tidal disruption distances have no meaning for close encounters between planets and small bodies with no rings or satellites.

$R_{\rm td}$ can be approximated as the secondary-primary body separation at which a satellite orbiting the secondary body would lie at the outer edge of the secondary body's Hill sphere. $R_{\rm radial}$ in Equation (2) is then by definition $R_{\rm td}$, and R_H is approximated by a_B. Solving for $R_{\rm td}$ yields

$$R_{\rm td} \approx a_B \left(\frac{3M_p}{m_s + m_{\rm sat}} \right)^{\frac{1}{3}} \tag{3}$$

(e.g., Philpott et al. 2010). Closer still to the primary body, the Roche limit is the distance from the primary within which a secondary body held together only by gravity would be torn apart by tidal forces. For a rigid secondary body, the equation for the Roche limit with respect to a primary body is approximately

$$R_{\rm roche} = 2.44 R_p \left(\frac{\rho_p}{\rho_s} \right)^{\frac{1}{3}} \tag{4}$$

(Roche 1849; Murray & Dermott 1999). Here, R_p is the physical radius of the primary body, ρ_p is the density of the primary body, and ρ_s is the density of the secondary body.

Now that a severity scale for close encounters has been established, it can be used to study simulated close encounters between ringed Centaurs and the giant planets.

4. The Two Dynamical Classes of Centaurs

Throughout its lifetime as a Centaur, the frequency and severity of close encounters between Chiron and the giant planets will affect the stability of any ring structure around Chiron. The frequency of close encounters can be affected by a Centaur's so-called dynamical class.

Previously it was shown that small bodies including Centaurs can be classified based on their perihelion, aphelion, and Tisserand parameter (as detailed in Horner et al. 2003).

However, as Bailey & Malhotra (2009) showed, Centaurs may also be classified into one of two classes based on their long-term dynamical behavior. The first type consists of those Centaurs that randomly wander from orbit to orbit. The semimajor axes of these Centaurs' orbits increase and decrease in time with no particular pattern. These Centaurs are known as random-walk Centaurs.

Centaurs of the other type spend most of their time temporarily trapped in mean motion resonances of the giant planets and typically jump from one resonance to the other. A small body is in a mean motion orbital resonance with a planet if the ratio of the orbital period of the planet to the orbital period of the small body equals a ratio of two small integers (Murray & Dermott 1999).

Becoming temporarily trapped in a resonance is a behavior known as resonance sticking (Lykawka & Mukai 2007). While trapped in a resonance, the semimajor axes of these Centaurs' orbits oscillate about a constant value which corresponds to the resonance location. These Centaurs are known as resonance hopping Centaurs. Since it is possible that resonance sticking can protect small bodies from close encounters with planets (Malhotra 1995), the dynamical class of a Centaur can have consequences for any ring structure around it.

The two types can also be more rigorously defined mathematically. As the semimajor axes of random-walk Centaurs wander aimlessly and those of resonance hopping Centaurs remain more constant, we would expect that on average the standard deviation of semimajor axis values of random-walk Centaurs would increase in time more predictably than those of resonance hopping Centaurs.

Mean standard deviation, then, can be used as a tool to distinguish between the two dynamical types. Random-walk Centaurs are those Centaurs whose mean square standard deviation of semimajor axis, $\langle \sigma^2 \rangle$, varies as a power law in time. It is said that these Centaurs display generalized diffusion. This can be expressed mathematically as

$$\langle \sigma^2 \rangle = Dt^{2H}. \tag{5}$$

Here, t is time, D is the generalized diffusion coefficient, and H is the Hurst exponent with $0 < H < 1$. Random-walk Centaurs can then be generally defined as those Centaurs for which the semimajor axis behavior is well described by generalized diffusion. Conversely, it then goes that the behavior of the semimajor axis of resonance hopping Centaurs is not well described by generalized diffusion.

Centaurs of both types may also display both random walking and resonance sticking during their lifetime. To determine if a Centaur is in fact trapped in a particular mean motion resonance, care must be taken.

Resonances do not exist at a single point but have widths in phase space. For example, for any particular resonance, a Centaur can be trapped in the resonance over a range of semimajor axis values.

To positively determine if a small body is trapped in a resonance, two behaviors must be displayed. First, the semimajor axis of the small body orbit must oscillate about the resonance location, and second, the primary resonance angle must librate in time (Smirnov & Shevchenko 2013).

The primary resonance angle is defined by $p\lambda - q\lambda_p - (p - q)\bar{\omega}$, where p and q are integers, λ_p is the mean longitude of the planet's orbit, λ is the mean longitude of the small body's orbit, and $\bar{\omega}$ is the longitude of perihelion of the small

body's orbit (Murray & Dermott 1999; Roig et al. 2002; Bailey & Malhotra 2009; Smirnov & Shevchenko 2013).

This angle is related to the perturbation of the orbit of a small body around a central body (like the Sun) by a third body (like a planet) in the planar 3-body problem. The reader is referred to Murray & Dermott (1999) for details.

5. Method

To study the dynamical history of Chiron and its ring system, a suite of numerical integrations were performed using the *n*-body dynamics package MERCURY (Chambers 1999).

A total of 35,937 massless clones of Chiron were integrated backward in time for 100 Myr in the six-body problem (Sun, four giant planets, and clone). The integration time is justified, as it is at least 100 times longer than the approximate half-life of Chiron (Hahn & Bailey 1990; Horner et al. 2004a).

The orbital elements of the individual clones were chosen from a range of three standard deviations below to three standard deviations above the accepted value of each orbital parameter of Chiron for epoch 2457600.0 JD taken from the Asteroid Dynamic Site (Knezevic & Milani 2012).

To create our cloud of clones for Chiron, we varied each of the orbital elements as follows. First, we sampled the $\pm 3\sigma$ uncertainty range in semimajor axis, a. We tested 11 unique values of the semimajor axis, ranging from $a - 3\sigma$ to $a + 3\sigma$, in even steps. At each of these unique semimajor axes, we tested 11 orbital eccentricities, which were again evenly distributed across the $\pm 3\sigma$ uncertainty in that variable. At each of these $121a - e$ pairs, we tested 11 unique inclinations also evenly spaced in the range $\pm 3\sigma$. This gave a grand total of 1331 potential $a - e - i$ combinations for Chiron. At each of these values, we tested 27 unique combinations of Ω, ω, and M, creating a $3 \times 3 \times 3$ grid in these three elements. The three values chosen for each of these three variables were the best-fit solution, and the two values separated by 3σ from that value. In total, this gave us a sample of 35,937 unique orbital solutions for Chiron.

The time step was chosen to be 40 days, which is approximately one-hundredth of an orbital period of Jupiter —the innermost planet included in this study. Similar time steps have been used before in integrations of both Centaurs and Main Belt asteroids (Tsiganis et al. 2000; Tiscareno & Malhotra 2003).

Clones were removed from the simulation upon colliding with a planet, colliding with the Sun, achieving an orbital eccentricity $\geqslant 1$, or reaching a barycentric distance >1000 au.

The masses and initial orbital elements of the four giant planets were found using the NASA JPL HORIZON ephemeris[8] for epoch 2451544.5 JD. Inclinations and longitudes for both Chiron and the planets were relative to the ecliptic plane.

In order to set their starting orbital parameters for the simulation, the planets were integrated (within the heliocentric frame) to the epoch 2457600.0 JD—the epoch of the Chiron clones using the *Hybrid* integrator within the MERCURY *n*-body dynamics package (Chambers 1999). The accuracy parameter was set to 1.d-12, and the hybrid handover radius was set to 3 Hill radii.

[8] https://ssd.jpl.nasa.gov/horizons.cgi?s_body=1#top (accessed 2015 December 31).

Table 3
Some Different Small Body Populations of the Solar System

Name	Definition
Inner SS	$a \leqslant a_J$
SP Comet	$a > a_J$ and $q < a_J$
Centaur	$a_J < a < a_N$ and $q > a_J$
TNO	$a \geqslant a_N$
Ejection	$e \geqslant 1$

Note. Here, a is the semimajor axis of the clone during the close encounter. The semimajor axis and other orbital values of the clone's orbit just before the close encounter were not recorded. a_J and a_N are the semimajor axis of Jupiter and Neptune, respectively; and q is the perihelion distance of the clone. Inner SS means inner solar system, SP comet means short period comet, TNO means trans-Neptunian object, and ejection means the clone was being ejected from the solar system at the time of the encounter.

Statistics on the close encounters were then taken by small body population of the solar system membership of the clone at the time of the encounter and by encounter severity. The different small body populations of the solar system used are defined in Table 3.

Physical properties of the planets were taken from NASA.[9] The mass of the Sun was also taken from NASA.[10] For Chiron we selected a bulk density of 1000 kg m^{-3}, which along with our selected radius of 90 km yielded a mass of 3.05×10^{18} kg. This mass was used in Equation (3) to determine the tidal disruption distance between Chiron and each planet. The density was used in Equation (4) to determine the Roche Limit between Chiron and each planet.

5.1. Determining the Half-life and Origin of Chiron

To determine the likely origin of Chiron, the chronologically earliest close encounter with a giant planet was analyzed for each clone, and the small body population of which the clone was a member at the time of the close encounter was found using the orbital parameters of the clone's orbit at the time of the encounter.

This then allowed the fraction of injection events from the various small body populations shown in Table 3 to be determined. (In other words, it allowed us to determine the likely source population of Chiron.)

Note that Trojans could overlap with the Centaur small body population the way we have defined it. However, in order to have a close encounter, a small body must have already exited the Trojan region.

Furthermore, though the Jupiter and Neptune Trojans are possible feeder populations to the Centaurs (e.g., Horner & Wyn Evans 2006; Horner & Lykawka 2010), our study is unable to yield any information on the likelihood of either of these being the source of Chiron. Therefore Trojans were omitted as separate populations in Table 3.

To determine the half-life of Chiron against removal from the simulation moving backward in time, the number of clones remaining at a time t was recorded as a function of time throughout the entire integration. Given N_o as the initial number of clones at a time $t = 0$, the half-life can be determined by fitting the data to the standard radioactive decay

[9] https://ssd.jpl.nasa.gov/?planet_phys_par (accessed 2017 June 16).
[10] https://nssdc.gsfc.nasa.gov/planetary/factsheet/sunfact.html (accessed 2017 June 17).

equation,

$$N = N_o e^{\frac{-0.693}{\tau}t}, \quad (6)$$

where τ is the half-life. The time interval over which the decay of clones was exponential was obtained by the fit of the data to Equation (6). Then the fit was used to calculate the half-life.

Once the half-life was determined, it was used in Equation (6) to determine the time at which 99.99% of clones would be removed from the simulation assuming a constant half-life. This time was then set as the upper limit on the time at which Chiron entered the Centaur region.

5.2. Finding the Dynamical Class

A separate set of integrations was made using the IAS15 integrator in the REBOUND n-body simulation package (Rein & Liu 2012; Rein & Spiegel 2015) using the orbital values from a set of 1246 Chiron clones from the previous integrations.

Three different samples of clones of ~400 clones each were used—the first sample was taken from the first 1000 clones, the second from the middle 1000 clones, and the third from the last 1000 clones in the entire data set. The middle sample included the currently accepted orbital values of Chiron.

It was not necessary to find the dynamical class of every clone, since the objective of these integrations is to compare and contrast the two dynamical classes and to explore specific examples of the behavior of clones in each class. Just a sampling of clones is sufficient for these purposes.

The output time was set to 300 years, and the time step was set to 0.1 year. In these integrations, clones were removed from the simulation upon colliding with the Sun, colliding with a planet, achieving an eccentricity $\geqslant 1$, or leaving the Centaur region. Any clone that did not remain in the Centaur region for at least 100,000 years was not used. The dynamical class of each remaining clone was found using the method of Bailey & Malhotra (2009):

1. Determine the time at which the clone was injected into the Centaur region, T_{Centaur}. Determine the number of data points in the time interval [0, T_{Centaur}].
2. Create a logarithmic interval of data points using [log (10), log(Data Points)].
3. Divide the interval into 16 equal logarithmic increments. Call the length of one of these increments j_s.
4. Create a window length of 10 data points in units of time. Set this equal to the smallest window length.
5. Create each z_{th} additional window length in units of data points, $w(z)_{\text{datapts}}$, by converting a logarithmic window into a window of data points using $w(z)_{\text{datapts}} = 10^{1+z(j_s)} + 1$ where $z \geqslant 1$.
6. Convert each window length from units of data points into units of time using $w(z)_{\text{time}} = w(z)_{\text{datapts}} \times$ (output time). The interval each window covers is closed on one end and open on the other. For example, the first window time interval would be [0, $w(z)_{\text{time}}$].
7. Discard any window lengths more than 25% of the data set.
8. Using the smallest window length, partition the time interval [0, T_{Centaur}] into equal windows of time and allow each window to overlap adjacent windows by half a window length.
9. Within each window, determine the standard deviation, σ, of the semimajor axis, a.
10. Calculate the mean standard deviation, $\bar{\sigma}$, over all windows.
11. Repeat the process for all the window lengths.
12. Perform a linear regression on $\log(\bar{\sigma})$ versus $\log(w(z)_{\text{time}})$.
13. The slope obtained from this regression is an approximation of the Hurst exponent.
14. A residual is the difference between an actual value and its expected value from the best-fit line. In this case, a residual of a particular value of $\log(\bar{\sigma})$ is found by finding the absolute value of the vertical distance from a value of $\log(\bar{\sigma})$ from the best-fit line. A Centaur is classified as being resonance hopping if the maximum value of any one residual is $\geqslant 0.08$. Otherwise, the Centaur is classified as random-walk. This method is based on the results of Bailey & Malhotra (2009), and the reader is referred to that work for more details.

Selected resonance hopping clones were studied in more detail by examining intervals of time in which the semimajor axis oscillated about a nearly constant value.

The semimajor axis values for these intervals of time were then smoothed using the technique of Hinse et al. (2010) to determine if the clone was trapped in a mean motion resonance of a giant planet. The method is as follows:

1. Qualitatively inspect graphs of semimajor axis versus time for resonance hopping Centaurs and identify intervals of time, ΔT_{res}, in which the semimajor axis seems to oscillate about a nearly constant value.
2. Select one of these intervals of time for study. Create a set of all semimajor axis data points during this time interval.
3. Initially, set the smoothed data set equal to the original data set.
4. By inspection, decide on a time window in units of data points. Set the window length to an odd number of data points and call this w_N.
5. Apply the window to the original data set at the first data point.
6. Evaluate the mean value of the semimajor axis over all data points within the window.
7. Set the value of the middle data point in this window (the $\boldsymbol{j}_{(w_N-1)\times 0.5}$ data point) in the smoothed data set to this mean value.
8. Slide the window ahead by one data point in the original data set and set the value of the middle data point in this window in the smoothed data set equal to the mean semimajor axis over the entire window in the original data set.
9. Continue this process until the window ends on the last data point. If j_{last} is the last data point, then in the smoothed data set the $j_{\text{last}} - j_{(w_N-1)\times 0.5}$ data point is set to the mean value of the semimajor axis in the window in the original data set. Any data points before the $\boldsymbol{j}_{(w_N-1)\times 0.5}$ data point and after the $\boldsymbol{j}_{\text{last}} - \boldsymbol{j}_{(w_N-1)\times 0.5}$ data point in the smoothed data set remain unchanged.
10. Try various window lengths until the smoothed data is as close to a cosine or sine wave in time as can be obtained by inspection.
11. Set the nominal location of the mean motion resonance equal to the mean value of the semimajor axis over the time interval ΔT_{res} in the smoothed data set.

12. Compare this location to known locations of mean motion resonances of the giant planets for identification. If the mean value is within 0.1 au of a resonance location, then consider that resonance as a possible candidate.
13. Examine the primary resonance angle associated with each candidate resonance for librating behavior over the time interval. If the angle librates, then consider the clone to be trapped in the resonance over the time of libration.

The locations of mean motion resonances of the giant planets, $a_{\rm res}$, were found using

$$a_{\rm res} = \left(\frac{j_1}{j_2}\right)^{\frac{2}{3}} a_p \tag{7}$$

(Murray & Dermott 1999). Here, a_p is the semimajor axis of a planet; and j_1 and j_2 are integers. In this work j_1 and j_2 were limited to values between 1 and 20.

5.3. MEGNO and Lifetime Maps

The chaoticity and chaotic lifetime of Chiron's orbital evolution were studied by means of calculating global MEGNO and lifetime maps over a given parameter region. The MEGNO (Mean Exponential Growth of Nearby Orbits; Cincotta & Simó 2000; Goździewski et al. 2001; Cincotta et al. 2003; Giordano & Cincotta 2004; Hinse et al. 2010) factor is a quantitative measure of the degree of chaos and has found wide-spread applications within problems of dynamical astronomy. The time averaged MEGNO parameter, $\langle Y \rangle$, is related to the maximum Lyapunov Characteristic Exponent, γ, by

$$\langle Y \rangle = t\frac{\gamma}{2} \tag{8}$$

as $t \to \infty$. For more on Lyapunov characteristic exponents, we direct the interested reader to Whipple (1995).

The detection of chaotic dynamics is always limited to the integration time period. Quasi-periodic or regular motion could in principle develop into chaotic motion over longer timescales. The calculation of $\langle Y \rangle$ involves the numerical solution of the associated variational equations of motion.

Following the definition of MEGNO, the quantity $\langle Y \rangle$ asymptotically approaches 2.0 for $t \to \infty$ if the orbit is quasi-periodic. For chaotic orbits, $\langle Y \rangle$ rapidly diverges far from 2.0. In practice, the limit $t \to \infty$ is not feasible and $\langle Y \rangle$ is only computed up to the integration time (eventually ended by some termination criterion such as the event of an escape or collision).

A MEGNO map is created using the technique of numerical integration of a number of massless test particles starting on initial orbits which cover a rectangular grid in $a - e$ space, with other orbital parameters held constant. In this work, the Gragg–Bulirsh–Stöer (Hairer et al. 1993) method was used to integrate 300,000 test particles for 1 Myr in the region of $a - e$ space bound by 13 au $\leqslant a \leqslant$ 14 au and $0 \leqslant e \leqslant 0.5$. The other orbital parameters were set to those of Chiron.

The resolution of the map was 600 × 500 ($a - e$). One test particle was integrated for each $a - e$ pair, for a total of 300,000 $a - e$ pairs.

The time step varied and was determined using a relative and absolute tolerance parameter, both of which were set to be close to the machine precision. A test particle was removed from the simulation if it collided with a planet or the Sun, was ejected from the solar system, or if $\langle Y \rangle > 12$ (indicating a strong degree of chaos).

When a test particle was removed, the time of removal and the $\langle Y \rangle$ value were recorded. If a test particle survived the entire simulation, then its removal time was recorded as 1 Myr. We will call the removal time the "chaotic lifetime," which is not the same as dynamical lifetime. However, it can be said that the dynamical lifetime is equal to or greater than the chaotic lifetime.

A chaotic lifetime map was then generated in conjunction with the MEGNO map by color-coding the lifetimes in the same $a - e$ grid used to create the MEGNO map. In the lifetime map the shortest removal times were color-coded black and the longest yellow. The resulting lifetime and MEGNO maps can be seen in Figures 7 and 8, respectively.

Table 4
Percentage of First Close Encounters by Clone Small Body Population Membership

Region	% CE
Inner SS	1
SP Comet	2
Centaur	2
TNO	60
Ejection	34

Note. The TNO population has the highest percentage of first close encounters, making it the most likely source population of Chiron.

6. Results

6.1. Half-life and Origin of Chiron

The percentage of first close encounters by clone small body population membership is shown in Table 4. The TNO population has the highest percentage of first close encounters, making it the most likely source population of Chiron.

Thirty-four percent of clones were in a hyperbolic or parabolic orbit during their first close encounter, which indicates a potential origin within the Oort cloud. The Centaur and Inner solar system populations combined contributed just 3% of the first close encounters.

The short period comet population claims 2% of first close encounters. These three populations combined likely illustrate potential final destinations for Chiron in the future, since dynamical evolution that takes no account of the influence of non-gravitational forces is entirely time-reversible.

Figure 1 shows the natural log of the fraction of remaining clones versus time over the last 2.5 Myr. The decay is exponential for the time interval [0.12 Myr, 0.5 Myr]. By 1 Myr ago, the decay curve departs markedly from this initial exponential decay.

This is typical and results from clones that have evolved onto more stable orbits. Because of this, these clones are no longer sampling the original phase space at the start of the decay.

To maximize the fit, the half-life during the exponential decay was determined on the interval [0.12 Myr, 0.367 Myr] and found to be about 0.7 Myr. Other larger intervals were tried and yielded the same result. This value is comparable to, but slightly shorter than, the value of 1.07 Myr reported by Horner et al. (2004b) for this quantity.

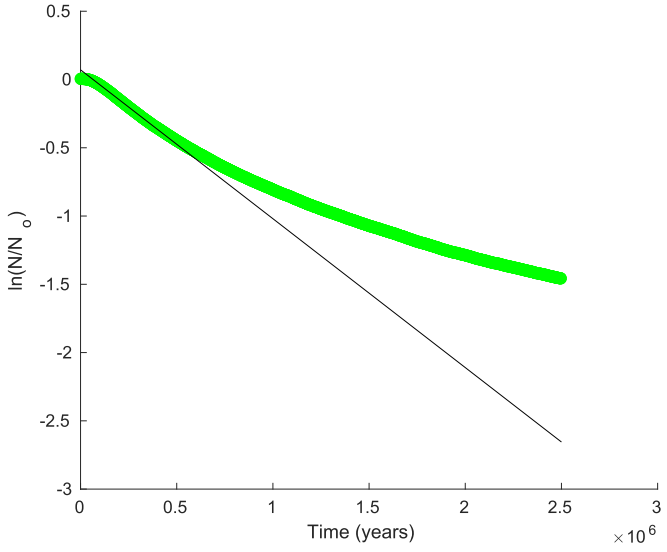

Figure 1. Natural log of the fraction of remaining clones versus time over the last 2.5 Myr. The decay is exponential through the interval [0.12 Myr, 0.50 Myr]. The half-life during the interval [0.12 Myr, 0.367 Myr] was found to be about 0.7 Myr. The solid line is the best-fit line for this interval and fits the data with a linear regression coefficient of 0.9999. By 1 Myr ago, it can be seen that the decay is no longer exponential.

Our smaller value is not surprising because Horner et al. (2004b) found their half-life using the longer time interval of 3 Myr, which included a longer tail over which the half-life was markedly different from its initial value.

A total 786 clones, just 2% of the total population, survived the entire integration time. Ninety-six percent of clones were ejected from the solar system on hyperbolic or parabolic orbits, which again points to an origin for Chiron beyond Neptune. Approximately 1% hit Jupiter, and the remaining 1% hit the Sun, Saturn, Uranus, or Neptune.

Using the best-fit line, we find that if the decay had remained exponential, then 99.99% of the clones would have been gone by 8.5 Myr ago. We use this time as the upper limit to the time at which Chiron first entered the Centaur region.

6.2. Close Encounters

The total number of close encounters between Chiron clones and the giant planets was 24,196,477. A total of 15,130,506 of these occurred while clones were in the Centaur region.

During their time in the Centaur region, clones experienced a close encounter on average every 5 kyr. Table 5 shows the number of these close encounters by planet.

As expected, clones had the highest numbers of close encounters with Saturn and Uranus, followed by Neptune and then Jupiter.

Table 6 lists the percentage of close encounters which occurred in the Centaur region by severity. It can be seen that the lower the severity, the greater the number of close encounters. There were only 48 severe and exactly zero extreme close encounters. These results show that encounters close enough to tidally disrupt Chiron or any ring system around Chiron are extremely rare events.

Thus it is unlikely that any ring structure around Chiron was created by tidal disruption due to a planetary close encounter, and barring ring dispersal by viscous spreading, it is possible that any ring structure around Chiron has survived its journey through the Centaur region and is in fact primordial.

Table 5
Close Encounters of Chiron Clones with Each Giant Planet while Clones Were in the Centaur Region

Planet	Number
Jupiter	553182
Saturn	6978716
Uranus	4567440
Neptune	3031168

Table 6
Percentage of Close Encounters of Chiron Clones with the Giant Planets by Severity while Clones Were in the Centaur Region

Severity	Percent
Very Low	89
Low	11
Moderate	0.03
Severe	0
Extreme	0

Table 7
Percentage of Clones and Mean Centaur Lifetime by Dynamical Class

Class	Percent	Avg. Centaur Life (Myr)
Resonance Hopping	5	1.1
Random-walk	95	0.52

Note. Random-walk dominates in quantity, but resonance hopping clones have about twice the mean centaur lifetime as random-walk clones due to resonance sticking.

6.3. Dynamical Class of Chiron

The dynamical classes of 1246 clones were determined. Table 7 shows the percentage of clones in each dynamical class, and the mean Centaur lifetime of clones in each class. Ninety-five percent of the sampled clones were classified as random-walk Centaurs, with the remaining 5% being classified as resonance hopping Centaurs.

The difference in mean Centaur lifetime between the two classes is stark. The mean Centaur lifetime for the resonance hopping clones was approximately twice as long as that of random-walk clones.

We hypothesise that the large difference is caused by resonance sticking in mean motion resonances of resonance hopping clones having the effect of prolonging their dynamical lifetimes. This is supported by the work of Bailey & Malhotra (2009). The top of Figure 2 shows the behavior of the semimajor axis of the orbit of one of the longest lived resonance hopping clones. In the figure, the semimajor axis spends about 5 Myr oscillating about the 2:3 mean motion resonance of Saturn centered at 12.5 au. Notice the horizontal band feature which covers this period of time. A shorter band centered at 15.1 au is caused by the exterior 1:2 mean motion resonance of Saturn.

Examination of other resonance hopping clones also showed relatively long periods of time for which each clone was trapped in one or more mean motion resonances. We conclude that resonance sticking acts to significantly prolong the lives of resonance hopping clones. Other notable resonances entered into by clones include the exterior 3:4, 4:7, and 1:3 resonances of Saturn; the Trojan or 1:1 resonance of Saturn; the interior 3:2

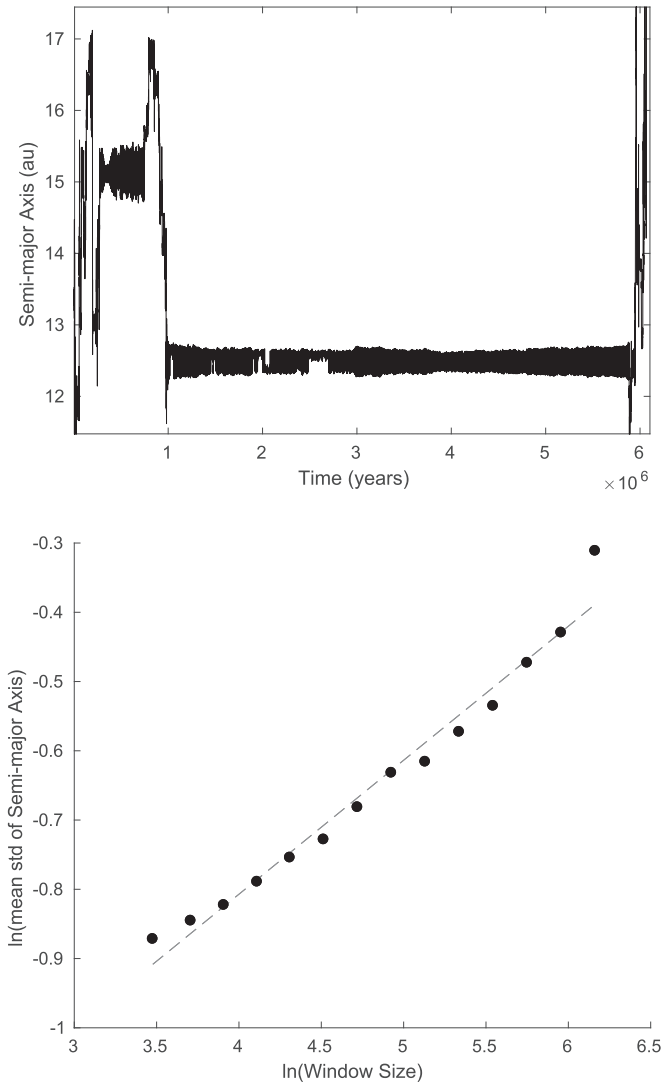

Figure 2. Top—an example of a resonance hopping clone. Note the long horizontal band feature. This clone spends about 5 Myr oscillating about the 2:3 mean motion resonance of Saturn located at 12.5 au. A shorter band centered at 15.1 au is caused by the exterior 1:2 mean motion resonance of Saturn. Bottom—the log–log plot used to identify the dynamical class of the clone in the top diagram. Notice the one data point at a larger distance from the trendline than the others. This is characteristic behavior for resonance hopping Centaurs. The Hurst exponent for this clone was 0.193, and its linear regression coefficient was 0.971. The maximum residual was 0.08.

resonance of Uranus; and the interior 3:2 and 4:3 resonances of Neptune.

The bottom diagram in Figure 2 shows the log–log plot used to classify the clone. It can be seen that it only takes one data point with a relatively large residual to cause a clone to be classified as resonance hopping.

The top diagram in Figure 3 shows another example of a resonance hopping clone. In contrast to the clone in Figure 2, which spends most of its time in one resonance, this clone spends most of its time hopping between mean motion resonances of the giant planets. Two of these resonances were positively identified as the 4:3 and 3:2 mean motion resonances of Neptune by observing the libration of their primary resonance angles.

The bottom diagram shows a close-up of the time spent in the 4:3 mean motion resonance of Neptune before and after data smoothing. The smoothed data set has a mean semimajor axis value that is only 0.07 au away from the 4:3 mean motion resonance of Neptune, located at 24.89 au.

Figure 4 shows the primary resonance angle associated with the 4:3 mean motion resonance of Neptune for the clone in Figure 3 over the same time interval. The angle is defined by $4\lambda_N - 3\lambda - \bar{\omega}$, where λ_N is the mean longitude of Neptune. It can be seen that this angle librates.

Figure 5 shows an example of a random-walk clone. This clone does not spend the majority of its life trapped in mean motion resonances, as can be seen by the lack of long horizontal bands in the figure.

The mean Hurst exponent of the random-walk clones is 0.4664 ± 0.0782, and that of the resonance hopping clones is 0.3572 ± 0.1530. Here the error is given by the standard deviation of the mean. It can be seen that Hurst exponents of random-walk clones are more well defined than those of resonance hopping clones, as the standard deviation of the mean of the Hurst exponents of random-walk clones is about half that of the resonance hopping clones.

Hurst exponents ranged from -0.1764 to 0.6416 for resonance hopping clones and from 0.1446 to 0.7462 for random-walk clones. The lowest regression coefficient for a random-walk clone was 0.85, and resonance hopping clones had regression coefficients ranging from -0.33 to 0.99.

Bailey & Malhotra (2009) reported that random-walk Centaurs display Hurst exponents in the range 0.22–0.95. We found that only five of our random-walk clones had Hurst exponents outside this range—all of them <0.22.

Qualitative inspection showed that four of these five could be classified as resonance hopping Centaurs, as they spent the majority of their lives in mean motion resonances. The fifth clone displayed both random-walk and resonance hopping behavior, but spent most of its time experiencing random-walk evolution. The fit of that clone's log–log plot had a regression coefficient of only 0.85, which is more than three standard deviations away from the mean value of 0.9947 ± 0.0089 for random-walk clones.

Furthermore, the outliers also had another thing in common: of the total time spent in resonances, each spent the majority of that time in only one strong resonance and did not jump into any other strong resonances. An example of one of these five outliers is shown in Figure 6.

This particular clone spends 66% of its life in the 2:3 mean motion resonance of Saturn and never jumps to another strong resonance. It was classified as a random-walk clone because its residuals never exceeded 0.0601, but since it spent more time in a resonance than random walking, one could argue that this clone is resonance hopping even though our method classifies it as random-walk. The linear regression coefficient of its log–log plot was 0.88, and its Hurst exponent was 0.19.

We conclude that our results are in good agreement with those of Bailey & Malhotra (2009), but that our technique occasionally misclassifies a clone. A refinement of this technique may be to consider the regression coefficients as well as the residuals as part of the classification procedure.

For example, if the regression coefficient of a random-walk clone falls below some critical value, then the clone should be classified manually. That is, classify it using qualitative inspection of the clone's semimajor axis behavior over time. The exact critical value to use will be left open for now.

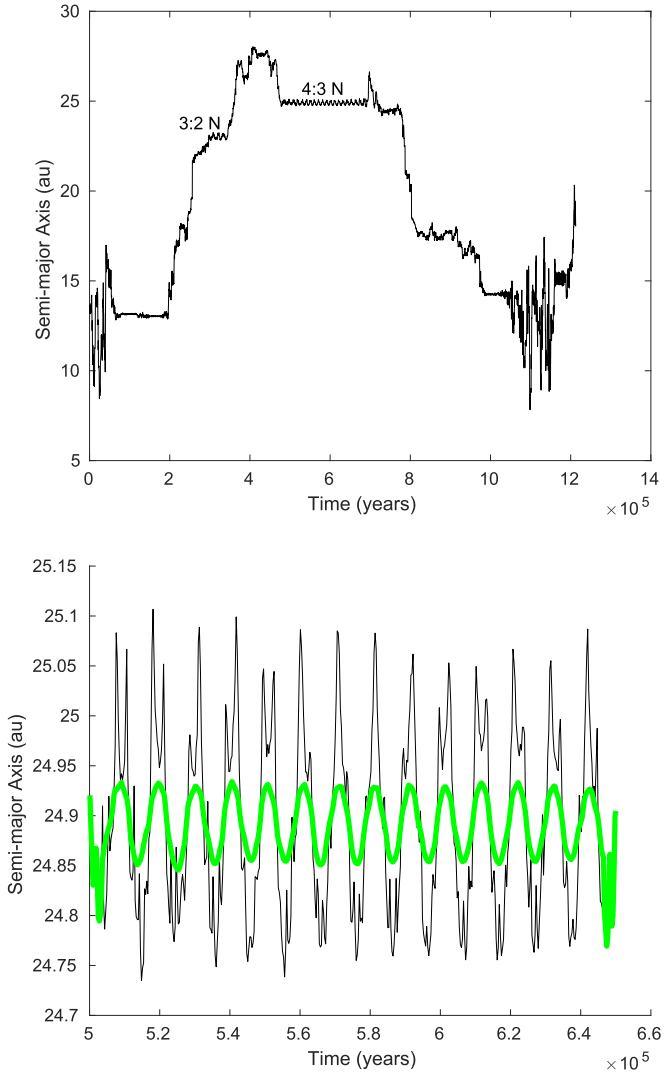

Figure 3. Top—another example of a resonance hopping clone. This clone spends most of its time trapped in various mean motion resonances of the giant planets. Two resonances were positively identified as the 4:3 and 3:2 mean motion resonances of Neptune. These are labeled in the figure. The Hurst exponent was 0.534, the linear regression coefficient was 0.9937, and the maximum residual was 0.08. Bottom—a close-up of the time spent in the 4:3 mean motion resonance of Neptune before and after data smoothing. The mean value of the smoothed data set was 24.89 au, which is about 0.07 au away from the 4:3 mean motion resonance of Neptune.

Another factor to consider is the distance of the Hurst exponent from the mean. All five of the outlying random-walk clones had Hurst exponents more than three standard deviations away from the mean. A refinement of the technique may be to manually classify any clones with outlying Hurst exponents. It remains to be seen if all outliers spend most of their lives in just one strong resonance or if this is just coincidental.

6.4. MEGNO and Lifetime Maps

Figure 7 shows the chaotic lifetimes of orbits in the region bound by 13 au $\leqslant a \leqslant$ 14 au and $0 \leqslant e \leqslant 0.5$. It can be seen that most orbits with $e \geqslant 0.23$ have lifetimes typically $\leqslant$0.01 Myr, which are noticeably shorter than the lifetimes of orbits of much lower eccentricity.

Chiron, located at the point (13.64 au, 0.38) lies in this region of relatively short lifetimes. Orbits with $a = 13$ au and

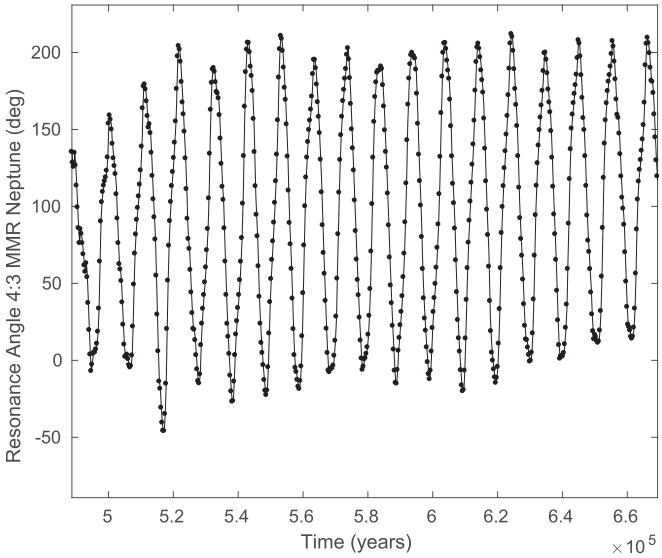

Figure 4. The primary resonance angle of the 4:3 mean motion resonance of Neptune defined by $4\lambda_N - 3\lambda - \bar{\omega}$ librates in time.

eccentricity of 0.23 just begin to cross the orbit of Saturn. All orbits with eccentricities above about 0.28 are Saturn crossing. This allows strong close encounters between objects on those orbits and the giant planet to occur immediately, which explains why most orbits with $e \geqslant 0.28$ have lifetimes $\leqslant$0.01 Myr—the lowest in the map.

One exception to this is the bump-like feature centered at 13.4 au, with a width of about 0.2 au. Orbits within the bump with eccentricities as high as 0.35 have lifetimes noticeably greater than 0.01 Myr.

For example, there are orbits in the bump with $e \geqslant 0.28$ with lifetimes of 0.1 Myr, which is an order of magnitude longer than most other orbits in the map with $e \geqslant 0.28$. Also of note is a cluster of orbits within the bump near $e = 0.1$, for which lifetimes can reach as high as 1 Myr—the longest in the map. We hypothesise that the bump feature is caused by resonance sticking in the 3:5 mean motion resonance of Saturn located at 13.4 au.

Small objects that get stuck in this resonance could have their chaotic lifetimes extended in the same way that the Centaur lifetime was extended for a clone stuck in the 2:3 mean motion resonance of Saturn, as seen in Figure 2. It should be noted, however, that most orbits located at 13.4 au with eccentricities below 0.06 have lifetimes noticeably shorter than 1 Myr.

This implies that small objects in this region of phase space are either not being captured in the resonance or are staying in the resonance for shorter times, which results in lower lifetimes. This may be caused by the decreasing width of the resonance for smaller eccentricities.

Such behavior of resonances has been seen before. For example, Murray & Dermott (1999) observed the same behavior for the 3:1 and 5:3 interior mean motion resonances of Jupiter located in the main asteroid belt.

Another bump of longer lifetimes that reach as high as 1 Myr is found between 13.9 and 14 au with $e \leqslant 0.05$. The low eccentricity of orbits in this bump help insulate them from destabilizing close encounters with Saturn and Uranus. Though their lifetimes of 1 Myr are relatively long compared to other orbits in the figure, this is still much shorter than the age of the

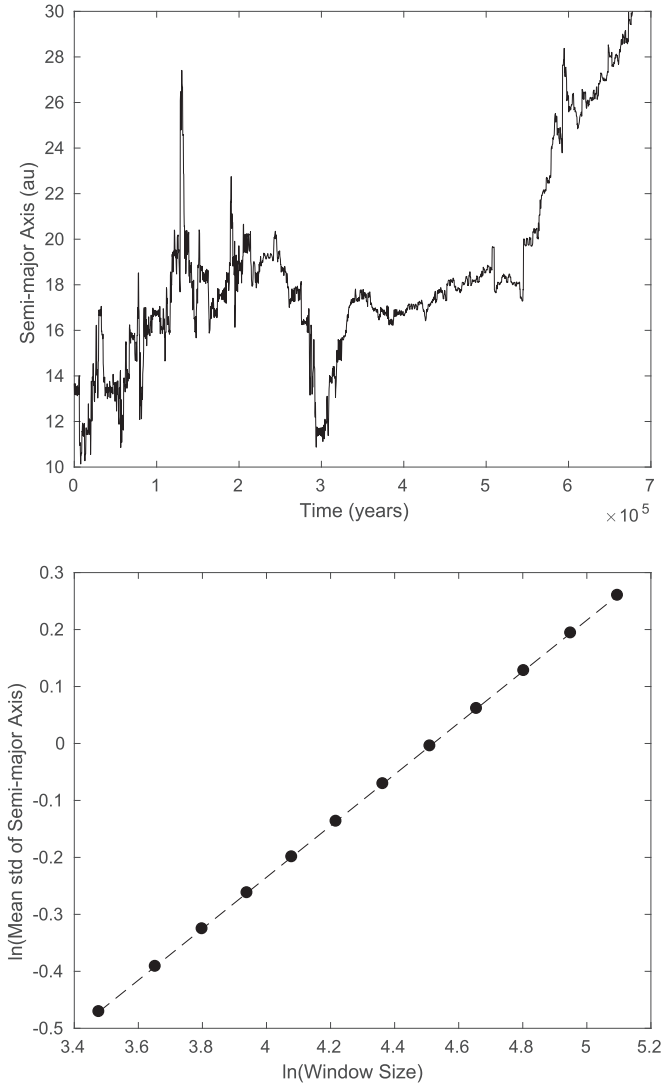

Figure 5. Top—an example of a random-walk clone. Notice how the long horizontal bands are absent. Bottom—the log–log plot used to identify the dynamical class of the clone in the top diagram. Notice the good fit. The linear regression coefficient was 0.9998, and the Hurst exponent for this clone was 0.4514. The maximum residual was 0.008.

solar system and so these orbits should be viewed as being only relatively stable.

Figure 8 is the MEGNO map of the same region of phase space. Almost the entire region, including the current orbit of Chiron, is highly chaotic. Two features of relatively lower chaos stand out: one island centered around 13.4 au with $0.1 \leqslant e \leqslant 0.15$ and a pair of islands between 13.9 and 14 au with $e < 0.04$. Here the MEGNO parameter reaches as low as 2.5. Two tinier islands can be seen between 13.7 and 13.9 au.

By comparison of the two maps, it can be seen that these islands are also embedded within regions of relatively long lifetimes that can reach as high as 1 Myr, making these islands regions of lower chaos and longer lifetimes.

It can also be seen that the two bumps of relatively long lifetimes found in the lifetime map also contain some orbits with lifetimes of 1 Myr that are also highly chaotic. Orbits that are chaotic but have a relatively long lifetime are said to display stable chaos.

Chiron, however, cannot be shown to display stable chaos, as it has a highly chaotic orbit and relatively short lifetime.

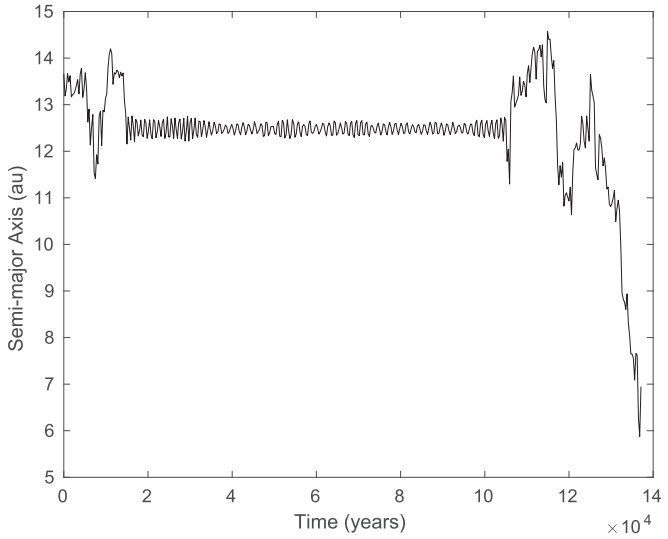

Figure 6. Random-walk clone that spent most of its life in the 2:3 mean motion resonance of Saturn located at 12.5 au. Though its residuals were $\leqslant 0.0601$, one could argue that it is a resonance hopping clone.

7. Conclusions

Using the technique of numerical integration of nearly 36,000 clones of the Centaur Chiron, we found the backward half-life of Chiron's orbit to be 0.7 Myr and showed that Chiron likely entered the Centaur region from somewhere beyond Neptune within the last 8.5 Myr.

Close encounters between Chiron and the giant planets severe enough to tidally disrupt Chiron or any ring system in a single pass were found to be extremely rare, and thus the origin of any ring structure is unlikely the result of tidal disruption of Chiron due to a planetary close encounter.

This led us to conclude that any supposed ring system around Chiron could be primordial barring ring dispersal by viscous spreading. Our results are similar to those of Wood et al. (2017) and Araujo et al. (2016) for the ringed Centaur Chariklo. In those studies, close encounters severe enough to severely damage or destroy the ring structure around Chariklo were also found to be very rare.

We also showed that the orbit of Chiron lies in a region of phase space that is both unstable and highly chaotic, and that the chaotic lifetime of Chiron is likely to be $\leqslant 0.01$ Myr. Resonance sticking was shown to have the ability to prolong the Centaur lifetime of Chiron clones by up to two orders of magnitude beyond its chaotic lifetime. Resonance sticking in the 2:3 exterior mean motion resonance of Saturn was cited as a strong example of this.

The dynamical classes of a sample of 1246 clones were determined while these clones were in the Centaur region. It was found that 95% of clones in the sample were categorized as random-walk Centaurs, and the remaining 5% were categorized as resonance hopping Centaurs. Because of resonance sticking, the mean Centaur lifetime of resonance hopping clones was about twice that of random-walk clones.

MEGNO and lifetime maps were made of the region in phase space bound by 13au $\leqslant a \leqslant$ 14au and $e \leqslant 0.5$, which included the orbit of Chiron. It was found that nearly the entire region is highly chaotic, with relatively small islands of lower chaos. Other small islands of stable chaos (high chaos and relatively long lifetime) were found.

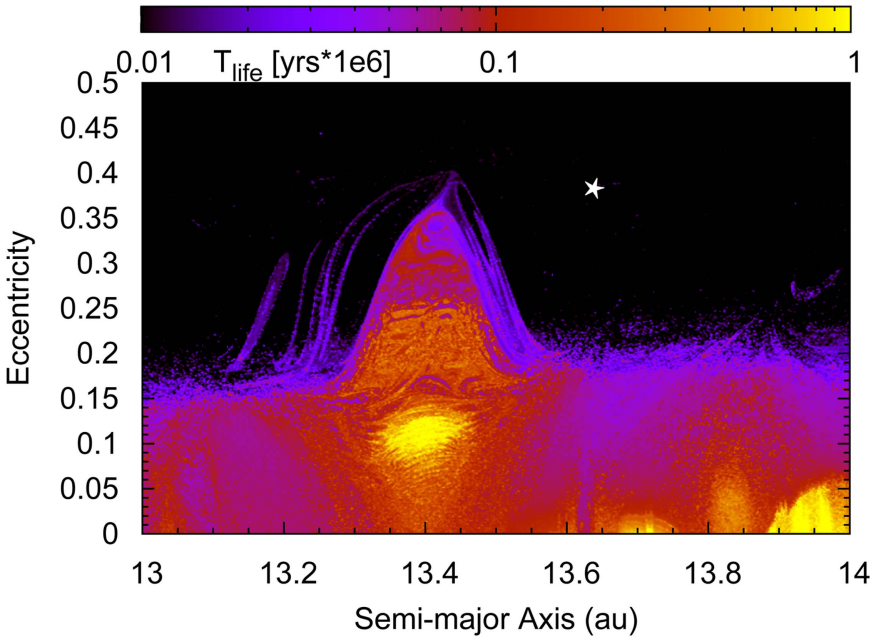

Figure 7. Chaotic lifetime map in $a - e$ space. Chaotic lifetime is the time to be removed from the simulation and not dynamical lifetime. However, the dynamical lifetime is greater than or equal to the chaotic lifetime. Chiron is shown as the star at the point (13.64 au, 0.38). A feature that stands out is the bump centered at 13.4 au, which has a width of about 0.2 au and a height of about 0.35. We hypothesize that the cause of the bump is resonance sticking in the 3:5 mean motion resonance of Saturn, which prolongs the lifetimes of test particles that get trapped in the resonance. A smaller bump can be seen between 13.9 and 14 au with $e \leqslant 0.05$. There is also a tiny bump in lifetimes up to 1 Myr between 13.7 and 13.75 au.

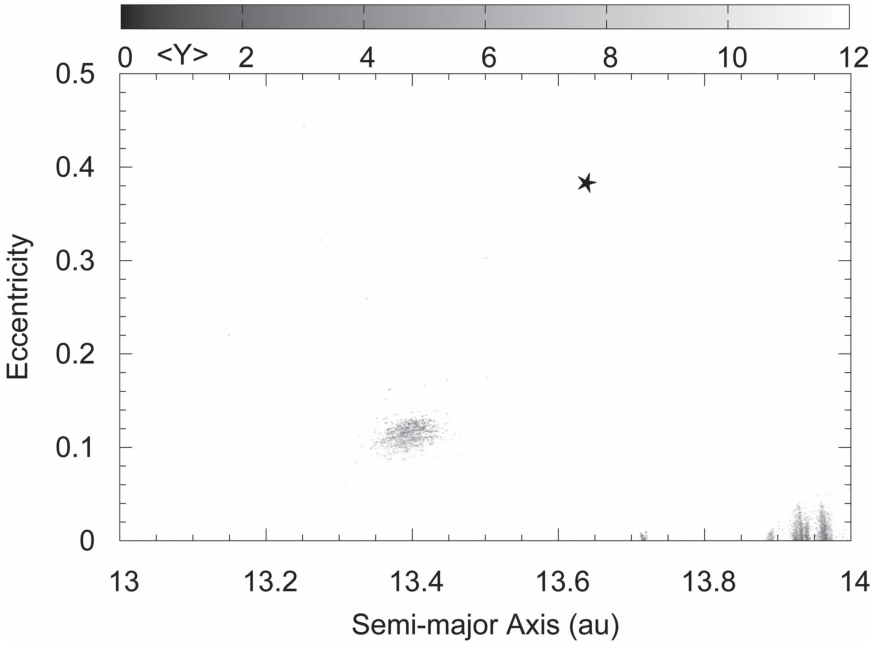

Figure 8. MEGNO map in $a - e$ space. Chiron is shown as the star at the point (13.64 au, 0.38). Nearly the entire region is highly chaotic. There are a few small islands of orbits with relatively low chaos. One is centered near 13.4 au with $0.1 \leqslant e \leqslant 0.15$, where the MEGNO parameter can reach as low as 3.5. Two others can be seen between 13.9 and 14 au, in which the MEGNO parameter reaches as low as 2.5. Two tinier islands can be seen between 13.7 and 13.9 au.

Most orbits with eccentricities $\geqslant$0.28 had the lowest chaotic lifetimes in the map of $\leqslant$0.01 Myr due to the crossing of Saturn's orbit. However, some test particles in orbits with $e \geqslant 0.28$ and semimajor axes within about 0.1 au of the exterior 3:5 mean motion resonance of Saturn located at 13.4 au were shown to have lifetimes up to 0.1 Myr, even for orbits with eccentricities up to about 0.35.

More research is needed to determine conclusively if the structure around Chiron is a ring system. It is not known if rings around small bodies are rare or commonplace. If future discoveries reveal that ringed Centaurs are common, it would suggest a common mechanism for the creation of the rings.

If, on the other hand, ringed Centaurs are found to be rare, then this would suggest a more serendipitous origin for rings. The authors encourage more searches for rings around other small bodies to help answer this question.

Thanks to the referee for their input on this work. Part of the numerical simulations were performed using a high performance computing cluster at the Korea Astronomy and Space Science Institute. T.C.H. acknowledges KASI grant #2016-1-832-01 and #2017-1-830-03.

ORCID iDs

Jeremy Wood https://orcid.org/0000-0003-1584-302X
Jonti Horner https://orcid.org/0000-0002-1160-7970
Tobias C. Hinse https://orcid.org/0000-0001-8870-3146

References

Araujo, R. A. N., Sfair, R., & Winter, O. C. 2016, ApJ, 824, 80
Bailey, B. L., & Malhotra, R. 2009, Icar, 203, 155
Braga-Ribas, F., Sicardy, B., Ortiz, J. L., et al. 2014, Natur, 508, 72
Brasser, R., Schwamb, M. E., Lykawka, P. S., & Gomes, R. S. 2012, MNRAS, 420, 3396
Bus, S. J., Buie, M. W., Schleicher, D. G., et al. 1996, Icar, 123, 478
Chambers, J. E. 1999, MNRAS, 304, 793
Chiang, E., Lithwick, Y., Murray-Clay, R., et al. 2007, in Protostars and Planets V, ed. B. Reipurth, D. Jewitt, & K. Keil (Tucson, AZ: Univ. Arizona Press), 895
Cincotta, P. M., Giordano, C. M., & Simó, C. 2003, PhyD, 182, 151
Cincotta, P. M., & Simó, C. 2000, A&AS, 147, 205
de la Fuente Marcos, C., & de la Fuente Marcos, R. 2014, Ap&SS, 352, 409
Di Sisto, R. P., & Brunini, A. 2007, Icar, 190, 224
Dones, L., Levison, H. F., & Duncan, M. 1996, in ASP Conf. Ser. 107, Completing the Inventory of the Solar System, ed. T. W. Rettig & J. M. Hahn (San Francisco, CA: ASP), 233
Duffard, R., Lazzaro, D., Pinto, S., et al. 2002, Icar, 160, 44
Elliot, J. L., Kern, S. D., Clancy, K. B., et al. 2005, AJ, 129, 1117
Elliot, J. L., Olkin, C. B., Dunham, E. W., et al. 1995, Natur, 373, 46
El Moutamid, M., Kral, Q., Sicardy, B., et al. 2014, in AAS Meeting 45 Abstracts, 402.05
Emel'yanenko, V. V., Asher, D. J., & Bailey, M. E. 2005, MNRAS, 361, 1345
Fornasier, S., Lellouch, E., Müller, T., et al. 2013, A&A, 555, A15
Fouchard, M., Rickman, H., Froeschlé, C., & Valsecchi, G. B. 2014, Icar, 231, 99
French, R. G., McGhee, C. A., Dones, L., & Lissauer, J. J. 2003, Icar, 162, 143
Giordano, C. M., & Cincotta, P. M. 2004, A&A, 423, 745
Gladman, B., Marsden, B. G., & Vanlaerhoven, C. 2008, in The Solar System Beyond Neptune, ed. M. A. Barucci et al. (Tucson, AZ: Univ. Arizona Press), 43
Goździewski, K., Bois, E., Maciejewski, A. J., & Kiseleva-Eggleton, L. 2001, A&A, 378, 569
Groussin, O., Lamy, P., & Jorda, L. 2004, A&A, 413, 1163
Hahn, G., & Bailey, M. E. 1990, Natur, 348, 132
Hairer, E., Nørsett, S. P., & Wanner, G. 1993, Solving Ordinary Differential Equations I, Vol. 8 (Berlin: Springer)
Hinse, T. C., Christou, A. A., Alvarellos, J. L. A., & Goździewski, K. 2010, MNRAS, 404, 837
Horner, J., Evans, N. W., & Bailey, M. E. 2004a, MNRAS, 354, 798
Horner, J., Evans, N. W., & Bailey, M. E. 2004b, MNRAS, 355, 321
Horner, J., Evans, N. W., Bailey, M. E., & Asher, D. J. 2003, MNRAS, 343, 1057
Horner, J., & Lykawka, P. S. 2010, MNRAS, 402, 13
Horner, J., Lykawka, P. S., Bannister, M. T., & Francis, P. 2012a, MNRAS, 422, 2145
Horner, J., Marshall, J. P., Wittenmyer, R. A., & Tinney, C. G. 2011, MNRAS, 416, L11
Horner, J., Müller, T. G., & Lykawka, P. S. 2012b, MNRAS, 423, 2587
Horner, J., & Wyn Evans, N. 2006, MNRAS, 367, L20
Hyodo, R., Charnoz, S., Genda, H., & Ohtsuki, K. 2016, ApJL, 828, L8
Jacobson, R. A., & French, R. G. 2004, Icar, 172, 382
Jewitt, D. 2009, AJ, 137, 4296
Jewitt, D. C. 2004, in Comets II, ed. M. C. Festou, H. U. Keller, & H. A. Weaver (Tucson, AZ: Univ. Arizona Press), 659
Knezevic, Z., & Milani, A. 2012, IAU Joint Discussion, 7, P18
Kovalenko, N. S., Babenko, Y. G., & Churyumov, K. I. 2002, EM&P, 90, 489
Kovalenko, N. S., Churyumov, K. I., & Babenko, Y. G. 2011, AstSR, 7, 230
Kowal, C. T., Liller, W., & Marsden, B. G. 1979, in Dynamics of the Solar System, Vol. 81 (Dordrecht: Reidel), 245
Lazzaro, D., Florczak, M. A., Betzler, A., et al. 1996, P&SS, 44, 1547
Levison, H. F., & Duncan, M. J. 1997, Icar, 127, 13
Liller, W., Chaisson, L. J., & Marsden, B. G. 1977, IAUC, 3151, 2
Lykawka, P. S., & Horner, J. 2010, MNRAS, 405, 1375
Lykawka, P. S., & Mukai, T. 2007, Icar, 192, 238
Malhotra, R. 1995, AJ, 110, 420
Marsden, B. G. 1962, ASPL, 8, 375
Meech, K. J., Buie, M. W., Samarasinha, N. H., Mueller, B. E. A., & Belton, M. J. S. 1997, AJ, 113, 844
Melita, M. D., Duffard, R., Ortiz, J. L., & Campo-Bagatin, A. 2017, A&A, 602, A27
Michikoshi, S., & Kokubo, E. 2017, ApJL, 837, L13
Murray, C. D., & Dermott, S. F. 1999, Solar System Dynamics (Cambridge: Cambridge Univ. Press)
Noll, K. 1994, PlR, 14, 8
Oikawa, S., & Everhart, E. 1979, AJ, 84, 134
Ortiz, J. L., Duffard, R., Pinilla-Alonso, N., et al. 2015, A&A, 576, A18
Ortiz, J. L., Santos-Sanz, P., Sicardy, B., et al. 2017, Natur, 550, 219
Pál, A., Kiss, C., Horner, J., et al. 2015, A&A, 583, A93
Pan, M., & Wu, Y. 2016, ApJ, 821, 18
Philpott, C. M., Hamilton, D. P., & Agnor, C. B. 2010, Icar, 208, 824
Rein, H., & Liu, S.-F. 2012, A&A, 537, A128
Rein, H., & Spiegel, D. S. 2015, MNRAS, 446, 1424
Robertson, P., Horner, J., Wittenmyer, R. A., et al. 2012, ApJ, 754, 50
Roche, E. 1849, Academie des Sciences de Montpellier: Memoires de la Sectiondes Sciences, 1, 243
Roig, F., Nesvorný, D., & Ferraz-Mello, S. 2002, MNRAS, 335, 417
Ruprecht, J. D., Bosh, A. S., Person, M. J., et al. 2015, Icar, 252, 271
Scholl, H. 1979, Icar, 40, 345
Shi, J. C., & Ma, Y. H. 2015, MNRAS, 454, 3635
Silva, A. M., & Cellone, S. A. 2001, P&SS, 49, 1325
Smirnov, E. A., & Shevchenko, I. I. 2013, Icar, 222, 220
Sykes, M. V., & Walker, R. G. 1991, Sci, 251, 777
Tiscareno, M. S., & Malhotra, R. 2003, AJ, 126, 3122
Tsiganis, K., Varvoglis, H., & Hadjidemetriou, J. D. 2000, Icar, 146, 240
Volk, K., & Malhotra, R. 2008, ApJ, 687, 714
Whipple, A. L. 1995, Icar, 115, 347
Wierzchos, K., Womack, M., & Sarid, G. 2017, AJ, 153, 230
Williams, J. G., & Benson, G. S. 1971, AJ, 76, 167
Wittenmyer, R. A., Horner, J., & Tinney, C. G. 2012, ApJ, 761, 165
Wood, J., Horner, J., Hinse, T. C., & Marsden, S. C. 2017, AJ, 153, 245
Wood, J. R., Horner, J., Hinse, T., Marsden, S. & Swinburne University of Technology 2016, in AAS/DPS Meeting 48 Abstracts, 120.23